



Nanoscale

Reversible Assembly of Silica Nanoparticles at Water-Hydrocarbons Interfaces Controlled by SDS Surfactant

Journal:	<i>Nanoscale</i>
Manuscript ID	NR-ART-10-2021-006807.R1
Article Type:	Paper
Date Submitted by the Author:	12-Nov-2021
Complete List of Authors:	Mohammed, Sohaib; Cornell University, Civil and Environmental Engineering Kuzmenko, Ivan; Argonne National Laboratory, Advanced Light Source Gadikota, Greeshma; Cornell University,

SCHOLARONE™
Manuscripts

1
2
3
4
5
6
7
8
9
10
11
12
13
14
15
16
17
18
19
20
21
22
23

Reversible Assembly of Silica Nanoparticles at Water-Hydrocarbons Interfaces Controlled by SDS Surfactant

Sohaib Mohammed,¹ Ivan Kuzmenko² and Greeshma Gadikota^{1,}*

¹School of Civil and Environmental Engineering, Cornell University. Ithaca, New York 14853, United States

²Advanced Photon Source, Argonne National Laboratory, Lemont, Illinois 60439, United States

* Corresponding Author. Phone: +1 607-255-4796. E-mail: gg464@cornell.edu

1 Abstract

2 Achieving reversible and tunable assembly of silica nanoparticles at liquid-liquid interfaces is vital
3 for a wide range of scientific and technological applications including sustainable subsurface
4 energy applications, catalysis, drug delivery and material synthesis. In this study, we report the
5 mechanisms controlling the assembly of silica nanoparticles (dia. 50 nm and 100 nm) at water-
6 heptane and water-toluene interfaces using sodium dodecyl sulfate (SDS) surfactant with
7 concentrations ranging from 0.001 – 0.1 wt % using *operando* ultrasmall/small-angle X-ray
8 scattering, cryogenic scanning electron microscopy imaging and classical molecular dynamic
9 simulations. The results show that the adsorption and assembly of silica nanoparticles at water-
10 hydrocarbon interfaces can be tuned by controlling the concentrations of SDS. Silica nanoparticles
11 are found to: (a) dominate the interfaces in the absence of interfacial SDS molecules, (b) coexist
12 with SDS at the interface at low surfactant concentration of 0.001 wt% and (c) migrate toward the
13 aqueous phase at a high SDS concentration of 0.1 wt%. Energetic analyses suggest that the van
14 der Waals and electrostatic interactions between silica nanoparticles and SDS surfactants increase
15 with SDS concentration. However, the favorable van der Waals and electrostatic interactions
16 between the silica nanoparticles and toluene or heptane decrease with increasing SDS
17 concentration. As a result, the silica nanoparticles migrate away from the water-hydrocarbon
18 interface and towards bulk water at higher SDS concentrations. These calibrated investigations
19 reveal the mechanistic basis for tuning silica nanoparticle assembly at complex interfaces.

20 **Keywords:** Silica nanoparticles; SDS; emulsions; USAXS/SAXS; Cryo-SEM; MD simulations.

21

22

1 **1. Introduction**

2 Achieving tunable controls on the dispersion behavior of silica nanoparticles in water and
3 hydrocarbon environments is crucial for probing their migration, precipitation and scaling
4 behavior for emerging sustainable subsurface energy applications including CO₂ storage in
5 hydrocarbon-bearing reservoirs. The changes in the porosity and permeability in subsurface
6 geologic environments resulting from the migration, aggregation and precipitation of fine siliceous
7 matter remains largely unexplored in the context of harnessing reservoirs for fluid storage and
8 recovery. While the adsorption of surfactants on mineral or rock surfaces is known to be influenced
9 by nanoparticles,^{1, 2} the mechanisms underlying surfactant-induced assembly of silica
10 nanoparticles at water-hydrocarbon interfaces remain less explored. The ability to tune interfacial
11 tension for coalescing and stabilizing oil-in-water emulsions is crucial for energy efficient water-
12 hydrocarbon separations. Despite the presence of suspended silica nanoparticles in natural aqueous
13 environments,³ their influence on stabilizing oil-in-water emulsions has not been studied.

14 Furthermore, advances in the use of engineered silica nanoparticles to architect new matter
15 for applications related to catalysis,^{4, 5} drug delivery,^{6, 7} materials synthesis,^{8, 9} separation,^{10, 11}
16 sensors,¹² adsorption,¹³ enhanced oil recovery¹⁴ and food processing¹⁵ motivate us to develop
17 mechanistic insights into the assembly of silica nanoparticles at complex fluidic interfaces. For
18 example, Pickering emulsions have been used as polymerization vessels for preparing hollow
19 microcapsules and composites capsules.¹⁶ These materials are widely used in food, pharmaceutical
20 and cosmetic products. Advancing fundamental insights into the interfacial behavior and the
21 energetic interactions underlying the organization of silica nanoparticles and surfactants at
22 complex interfaces is crucial for synthesizing novel materials. With this context, the following
23 questions are addressed in this study: (i) What is the influence of surfactant concentrations on the

1 organization or displacement of silica nanoparticles at water-hydrocarbon interfaces? (ii) How
2 does the interfacial behavior of surfactants and silica nanoparticles evolve with the size of
3 nanoparticles? (iii) What are the energetic interactions underlying the organization or displacement
4 of silica nanoparticles away from water-hydrocarbon interfaces?

5 Prior experimental and computational studies utilized various techniques, including
6 Pendant drop tensiometer and molecular dynamics simulations¹⁷⁻²² to probe the interfacial
7 behavior of surfactants and nanoparticles at various water-hydrocarbon interfaces. While some
8 studies concluded that the synergetic interactions of nanoparticles and surfactants on the interface
9 enhance emulsion stability,²²⁻²⁷ others reported that the surfactant concentrations higher than the
10 critical micelle concentration leads to the displacement of the nanoparticles from the interface.²⁸
11 ²⁹ Although it is poorly understood, the mechanism governing the displacement of nanoparticles
12 from the interface is related to the interfacial tension of the associated emulsion and the contact
13 angle between the nanoparticles and the liquid phases.¹⁷

14 The energy required to displace a nanoparticle from the interface can be quantified as
15 $E = \pi r^2 \gamma_{ow} (1 \pm \cos \varphi)^2$ where r is the radius of the nanoparticle, γ_{ow} is the interfacial tension of
16 the oil-in-water emulsion, and φ is the contact angle of the adsorbed nanoparticles at the
17 interface.³⁰ The extent to which the nanoparticles adsorb at the interface depends on the wettability
18 of these nanoparticles. Nanoparticles with highly hydrophilic or hydrophobic surfaces tend to
19 disperse in water or hydrocarbons phases, respectively. According to the equation above, the
20 maximum energy required to displace a nanoparticle from the interface is at a contact angle of 90°.
21 The synergetic interactions of surfactants and nanoparticles on the interface can alter the wetting
22 properties of the assembled nanoparticles and eventually enhance or inhibit the assembly of

1 nanoparticles on the interface. Vashisth and co-workers²⁹ showed that adding high surfactant
2 concentrations can completely disrupt the assembly of nanoparticles from the interface because
3 the presence of the surfactant at the water-oil interface is energetically favored compared to
4 nanoparticles. This displacement was also attributed to the influence of the added surfactants on
5 the nanoparticle contact angle at the interface,^{31, 32} the extent of nanoparticle flocculation,^{33, 34} the
6 dynamics of nanoparticles at the interface³⁵ and the competitive assembly of surfactant molecules
7 at the interface.³⁶ Resolving the synergetic effects of surfactant and nanoparticles enables us to
8 tune the self-assembly behavior of nanoparticles at water-hydrocarbon interfaces in addition to the
9 ability to control the interfacial properties of the associated emulsion including the coalescence of
10 small drops into larger drops that facilitate the separation of water and oil phases.

11 In this study, we introduce an experimental and computational approach to elucidate the
12 interfacial behavior underlying the co-existence of silica nanoparticles with diameters of 50 nm
13 and 100 nm and sodium dodecyl sulfate (SDS) concentrations ranging from 0.001-0.1% at water-
14 heptane and water-toluene interfaces. Ultrasmall- and Small-Angle X-Ray Scattering
15 (USAXS/SAXS) measurements, Cryogenic Scanning Electron Microscopy (Cryo-SEM) imaging,
16 and Molecular Dynamics (MD) simulations are harnessed to probe the coexistence of hydrophilic
17 silica nanoparticles and SDS molecules on the interfaces and their influence on the interfacial
18 properties of the studied emulsions. The interfacial behavior of the silica nanoparticles is
19 investigated at SDS surfactant concentrations of 0.001, 0.01 and 0.1 wt%. The experiments and
20 simulations are performed at 1 bar and 298 K. This experimental and simulation approach enables
21 us to develop fundamental insights into the structure, dynamics and morphology of nanoparticles
22 and surfactants assembled at water-hydrocarbon interfaces across spatial and temporal scales.

23

1 **2. Methodology**

2 **2.1. Sample preparation**

3 Silica nanoparticles with diameters of 50 nm and 100 nm dispersed in Milli-Q water with
4 a concentration of 10 mg/mL (1 wt.%) purchased from nanoComposix, Inc are used. The sizes and
5 the dispersion states of the nanoparticles are confirmed by measuring the USAXS/SAXS
6 intensities of the solutions bearing nanoparticles prior to the preparation of the solutions. The
7 average size of the well dispersed nanoparticles is confirmed to be 51.35 ± 3.15 nm and $101.35 \pm$
8 4.17 nm using USAXS/SAXS measurements.³⁷ The suspensions of 50 nm and 100 nm
9 nanoparticles have a pH of 9.7 and 7.4, respectively. ζ potential of the 50 nm and 100 nm
10 nanoparticles suspensions are -51 mV and -59 mV, respectively. SDS surfactants are purchased
11 from Sigma-Aldrich and used without further treatment. SDS powder is dissolved in high purity
12 (99.9%) heptane and toluene solvents to produce solutions with SDS concentrations of 0.001 wt.%,
13 0.01 wt.%, and 0.1 wt.%. The SDS solutions are stirred at 800 rpm under 298 K for 2 hours to
14 ensure complete dissolution of the added surfactants. The water-heptane and water-toluene
15 interfaces are prepared by injecting 50 μ l of the nanoparticles' suspensions followed by 50 μ l of
16 the SDS solutions in a glass vial with a diameter of about 1 mm (see **Figure 1 (a)**). The emulsions
17 were left undisturbed at 298 K for 24 hours prior to characterization.

18 **2.2. Ultra-Small/Small Angle X-Ray Scattering (USAXS/SAXS) Measurements**

19 The assembly of silica nanoparticles and surfactants at the water-hydrocarbon interfaces
20 are determined using Ultra-Small/Small Angle X-Ray Scattering (USAXS/SAXS) measurements.
21 These measurements are performed by detecting the scattered X-ray beam from the interfaces of
22 the water-hydrocarbon emulsions on a 2D detector (see **Figure 1(a)**). The experiments are
23 conducted at sector 9-ID-C in the Advanced Photon Source (APS) at Argonne National

1 Laboratory.^{38, 39} The total X-ray flux is 10^{13} photon $\text{mm}^{-2} \text{s}^{-1}$. The energy of the incident X-ray
2 beam during the measurement is 21.0 keV that corresponds to a wavelength of 0.589 Å. The
3 scattered USAXS data are collected using a Bonse-Hart camera and the scattered SAXS data are
4 acquired using a pinhole camera on a Pilatus 100K detector (Dectris Ltd., Baden Switzerland). The
5 data acquisition times for the USAXS and SAXS measurements are 90 and 5 sec, respectively.
6 The 2D data are reduced and converted to 1D curves using the Nika (SAXS)⁴⁰ and Irena (USAXS)
7 ⁴¹ macros implemented in *Igor* software. The background scattering from the interfaces of water-
8 heptane and water-toluene emulsions free of surfactants and nanoparticles are collected and
9 subtracted from the scattering data. The wavevector (Q) values (where $Q = (4\pi/\lambda) \sin \theta$, λ is the
10 X-ray wavelength, and θ is one half of the scattering angle) and sample-to-detector distances (and
11 geometry) are calibrated using silver behenate. Additional information about the X-ray scattering
12 measurements is included in a prior publication by Mohammed and co-workers.³⁷

13 **2.3. Cryogenic Scanning Electron Microscopy (Cryo-SEM)**

14 Cryo-SEM imaging is performed using the FEI Strata 400S DualBeam instrument at the
15 Cornell Center for Materials Research (CCMR) for high-resolution and high-contrast imaging.
16 The prepared emulsions are frozen using liquid nitrogen to avoid changes in the interfacial
17 structure of the nanoparticles and surfactants. The freezing time of the studied emulsions is in the
18 order of milliseconds. Different regions at the water-heptane and water-toluene interfaces and in
19 the bulk water phase are imaged to visualize the morphology of nanoparticles at various SDS
20 concentrations.

21 **2.4. Molecular dynamics simulations**

1 Silica nanoparticle with a diameter of 3 nm is cleaved from a well-studied and validated β -
2 cristobalite unit cell. The size of the simulated nanoparticles is chosen for three main reasons: (a)
3 the ease of modifying the surface chemistry of these nanoparticles to reflect the density of OH
4 groups on the surface of the silica nanoparticles used in the experiment, (b) using 3 nm sized
5 nanoparticles allows us to use a concentration of 10 mg/mL (5 nanoparticles) in a reasonably large
6 simulation cell and (c) using 3 nm sized silica nanoparticles provide enables us to conduct the
7 simulations for reasonably sufficient simulation time (50 ns) to reach equilibrated states and draw
8 reasonable conclusions. Further, simulating larger sized nanoparticles requires adopting other
9 simulation techniques such as coarse-grained molecular dynamics (GCMD) and dissipative
10 particles dynamics (DPD) in which the atomic scale description of molecules is not considered.
11 For example, Yu and Zhou⁴² utilized CGMD to understand the curvature effect of silica
12 nanoparticles with diameters of 2 to 10 nm on the adsorption of lysozyme enzyme. Although the
13 size of silica nanoparticles used in the simulation is smaller than the nanoparticles used in the
14 experiments, the interfacial behavior and trends in the energetic interactions can be accurately
15 predicted.

16 The nonbridging surface oxygens on the nanoparticle's surface are functionalized with
17 hydroxyl (OH) groups with a surface density of about 7.3 OH/nm². The rationale behind choosing
18 this level of hydroxylation is driven by the chemistry of the nanoparticles used in the experiments
19 which are dominated by silanol groups (Si-OH) on the surface and the typical density of OH groups
20 on the silica surfaces used in previous studies.⁴³⁻⁴⁵ Further, our reactive molecular dynamics
21 simulations (ReaxFF) shows that nonbridging oxygens on the surface of 3 nm sized silica
22 nanoparticles undergo continuous hydroxylation when dissolved in 1 g/cm³ of water at 298 K and
23 1 bar (**see Figure S1 and S2**).

1 Five silica nanoparticles are randomly distributed in a 7 nm × 7 nm × 10 nm cell with a
2 concentration of 1 wt.% to match the experimental concentration of the silica nanoparticles
3 suspensions. The simulation cell is extended in the z-direction by 5 nm and SDS-heptane and SDS-
4 toluene mixtures are added with SDS concentrations of 0 wt.%, 0.001 wt. %, 0.01 wt. %, and 0.1
5 wt. % (see **Figure 1(b)**). The dimensions of the initial simulation cells are 7 nm x 7 nm x 15 nm
6 in *x*, *y* and *z* directions, respectively. Periodic boundary conditions are used in the *x*, *y* and *z*
7 directions.

8 Silica nanoparticles and water molecules are modeled using parameters from CLAYFF⁴⁶
9 and TIP4P⁴⁷, respectively, while heptane, toluene and SDS molecules are modeled using the
10 OPLS/AA forcefield^{48, 49} (see the forcefield parameters in **Table S1**). The combination of
11 OPLS/AA and CLAYFF forcefields have been used extensively in investigating the interactions
12 of hydrocarbons and surfactant with silica surfaces.⁵⁰⁻⁵² 50,000 steps of energy minimization using
13 “steepest descent” method are performed on the initial configurations to decrease their high energy
14 and remove the inappropriate geometries. The minimized configurations underwent semi-isotropic
15 compression in z-direction, the direction normal to the interface for 50 ns using the constant
16 number of molecules, constant pressure, constant interfacial area, and constant temperature
17 (NPAT) ensemble. The simulations are performed at 1 bar and 298 K to be consistent with the
18 experimental conditions. Nose-Hoover thermostat^{53, 54} with a relaxation time of 1 ps and
19 Parrinello–Rahman barostat⁵⁵ are used to maintain the required temperature and pressure. The
20 equation of motion is integrated using the leapfrog algorithm with a time step of 1 fs. The short-
21 range interactions are calculated within a cutoff of 1.4 nm, while the long-range electrostatic
22 interactions are treated using Particle Mesh Ewald (PME).⁵⁶ The nonbonded van der Waals and
23 electrostatic interactions are modeled using 12-6 Lennard-Jones and coulombic models,

1 respectively. The bonded interactions account for bonds stretching, angles bending and dihedrals,
2 except for silica nanoparticles where only OH bond stretching are accounted for. All the
3 simulations are conducted using GRONingen Machine for Chemical Simulations (GROMACS
4 2018) simulation package.⁵⁷

5 **3. Results and Discussions**

6 **3.1. Assembly of nanoparticles and SDS on the interfaces**

7 The assembly of silica nanoparticles and SDS molecules on water-heptane and water-
8 toluene interfaces is evident from the USAXS/SAXS intensity curves (**see Figure 2**). At 0 wt%
9 SDS, the scattering curves suggest that water-heptane and water-toluene interfaces are dominated
10 by 50 nm and 100 nm silica nanoparticles as the intensities shows a scattering pattern that
11 corresponds to that of spherical nanoparticles. The assembly behavior of silica nanoparticles with
12 comparable sizes at water-heptane and water-toluene interfaces under similar conditions are
13 evident from prior experimental and computational studies.^{37, 58} The scattering behavior from the
14 interfacial silica nanoparticles is observed in the presence of 0.001 wt.% SDS concentrations,
15 suggesting the coexistence of nanoparticles and surfactants on water-heptane and water-toluene
16 interfaces. Interestingly, as SDS concentrations increases to 0.01 wt.%, the scattering curve from
17 water-heptane interface indicates the dominance of silica nanoparticles, while the detected
18 intensity from water-toluene interfaces suggests that SDS molecules occupy the interfacial region
19 and displace the nanoparticles toward the aqueous phase. These results suggest that the higher
20 interfacial energy of water-heptane systems corresponds to an enhanced assembly of silica
21 nanoparticles.

1 As 0.1 wt.% SDS is added to the system, the water-heptane and water-toluene interfaces
2 are completely occupied by SDS molecules and no scattering from nanoparticles was observed,
3 suggesting that the interfacial nanoparticles are completely displaced from the interface and
4 emerged in the water phase. The competitive assembly of silica nanoparticles and SDS molecules
5 on water-hydrocarbon interfaces is consistent with prior experimental work showing that the small
6 quantities of surfactants stabilized nanoparticle emulsions.^{29, 59}

7 To determine the size distribution and the number of interfacial silica nanoparticles at
8 water-heptane and water-toluene interfaces, we analyzed the USAXS/SAXS data that represent
9 the scattering behavior of silica nanoparticles and surfactants at these interfaces. Quantitative
10 analyses on the nanoparticles' dominated interfaces are performed by modeling the structure factor
11 $S(\vec{Q})$ and the form factor $P(\vec{Q})$ of the intensity curves on the Q scale. The intensity $I(\vec{Q})$ scattered
12 from identical spherical nanoparticles can be expressed as the product of $S(\vec{Q})$ and $P(\vec{Q})$ such
13 that ⁶⁰:

$$14 \quad I(\vec{Q}) = S(\vec{Q})P(\vec{Q}) \quad (1)$$

15 The size distribution and the number of interfacial silica nanoparticles at water-heptane and
16 water-toluene interfaces (**Figure 3**) are obtained from fitting $P(\vec{Q})$ at the high Q regions. At 0 wt%
17 SDS, the number of 50 nm and 100 nm nanoparticles assembled at water-toluene surfaces is higher
18 compared to water-heptane interfaces. The number of 50 nm and 100 nm silica nanoparticles at
19 water-heptane and water-toluene interfaces decreased substantially as the SDS concentration
20 increased to 0.001 wt%, indicating that the added SDS molecules preferentially occupy the
21 interfacial area and thus reduce the available area for the nanoparticles to adsorb on the interface.

1 It is interesting to note that the number of interfacial silica nanoparticles at water-heptane interface
2 remains similar when the concentrations of surfactants are 0.001 wt% and 0.01 wt% irrespective
3 of the size of the nanoparticles (**Figures 3 (a) and 3 (c)**). In contrast, the number of silica
4 nanoparticles at the water-toluene interface dropped to zero on increasing the concentration of
5 surfactants to 0.01 wt% and 0.1 wt% (**Figures 3 (b) and 3 (d)**). These observations agree with the
6 findings of Vashisth and co-workers that interfacial surfactants displace the adsorbed nanoparticles
7 after accounting for the difference in the sizes of nanoparticles.²⁹

8 The observations noted from **Figure 3** are consistent with the scattering data shown in
9 **Figure 2**. The scattering pattern from water-heptane and water-toluene interfaces at high SDS
10 concentrations (i.e., 0.1 wt. % at water-heptane and ≥ 0.01 wt.% at water-toluene) suggests the
11 absence of silica nanoparticles at these interfaces and the dominance of surfactant assemblies (**see**
12 **Figure 2**). At 0.1 wt.% SDS, the scattering curves from the water-heptane interfacial regions
13 showed peaks at about 0.05 \AA^{-1} indicating scattering from self-assembled surfactants. The
14 scattering from self-assembled surfactants at water-toluene are noticed at 0.01 wt.% and at 0.1
15 wt.% SDS concentrations, whereas peaks are detected at about 0.031 \AA^{-1} and 0.026 \AA^{-1} ,
16 respectively. The locations of the peaks in water-heptane and water-toluene systems show the
17 dependence of the formed assemblies sizes and morphologies on the interfacial properties of the
18 corresponding emulsions. Porod analysis of the interfacial surfactants on water-heptane and water-
19 toluene interfaces are performed at high Q region to investigate the morphology of the self-
20 assembled SDS molecules (**see Figure 2**). The power law slope values of the scattering intensity
21 curves on water-heptane interfaces in the presence of 0.1 wt.% are 2.4 and 2.3 for emulsions with
22 50 nm and 100 nm silica nanoparticles, respectively. These values indicate the formation of 2D
23 disk-like morphologies by the interfacial surfactants. However, SDS molecules at the interfaces of

1 water-toluene forms both 2D disk-like (Q^{-2}) and 1D rod-like (Q^{-1}) morphologies. The formation of
2 surfactant ensembles on water-hydrocarbons interfaces are evident from prior experimental and
3 computational studies.⁶¹⁻⁶⁴ Czajka and Armes⁶¹ concluded that the presence of SDS surfactants
4 results in the formation of spherical latex emulsions based on SAXS measurements. Shi and Guo⁶⁴
5 performed MD simulations on the effect of SDS molecular structure on its aggregation
6 morphology at water-trichloroethylene interfaces. The results indicated that the surfactants form a
7 continuous monolayer at the interface as the interfacial coverage increases.

8 The morphology of the self-assembled silica nanoparticles and SDS ensembles are further
9 analyzed by calculating the power law slope in the USAXS (low Q) region (**see Figure 4**). The
10 morphology of self-assembled nanoparticles and SDS molecules change significantly with the
11 SDS concentration. The low power law slope (< 1) in the absence (0 wt.%) and presence of low
12 SDS concentrations (0.001 wt.%) indicate that the interfacial nanoparticles and SDS molecules are
13 well dispersed at the interfaces. As the SDS concentration increases, the power law slope values
14 increase substantially, implying the emergence of SDS aggregates with varying morphologies. A
15 power law slope of < 3 indicates the formation of surface fractals.^{65,66} Further, the displaced silica
16 nanoparticles to the bulk water are well dispersed with no indication of self-assembly as the power
17 low slope is < 1 in the USAXS region (**see Figure S3**).

18 The displacement of interfacial nanoparticles from water-heptane and water-toluene
19 interfaces are confirmed by cryo-SEM imaging (**see Figure 5**). At low SDS concentrations of
20 0.001 wt.%, the nanoparticles are abundant in the interfacial region of water-heptane and water-
21 toluene emulsions. The nanoparticles are mostly found as individual nanoparticles with minor
22 traces as aggregates on water-heptane and water-toluene interfaces (**see Figure 5 (a) and (c)**).
23 However, the number of interfacial nanoparticles on water-heptane and water-toluene interfaces

1 were significantly reduced as the SDS concentration increased to 0.1 wt.%. Only traces of
2 nanoparticles are observed at the interfaces due to the displacement into the aqueous phase by the
3 interfacial SDS assemblies. The cryo-SEM data agrees with the observation of USAXS/SAXS
4 scattering measurements (**Figure 2**).

5 Additional insights into the assembly of silica nanoparticles and SDS molecules on water-
6 heptane and water-toluene interfaces are obtained from the density profiles governed by MD
7 simulations (**Figure 6**). The density profiles are averaged over the last 10 ns of the simulation time
8 and calculated along the axis normal to the interface (z-axis). Water and hydrocarbons formed two
9 separated phases, while the silica nanoparticles and SDS molecules are dispersed in the water and
10 hydrocarbon phases, respectively, with favorable assembly at the interfaces (**Figure 6 (a) and (b)**).
11 The initially dispersed nanoparticles in the water phase migrated and assembled on the interfaces
12 to extents that differ with the concentration of SDS molecules. SDS density profiles showed peaks
13 at water-heptane and water-toluene interfaces, indicating preferential assembly at water-
14 hydrocarbon interfaces compared to the dispersion in bulk hydrocarbons. Higher peaks in SDS
15 profiles are observed on water-toluene interfaces compared to water-heptane interfaces.

16 Interestingly, the density profiles of silica nanoparticles at water-heptane interfaces showed
17 a systematic shift toward the water phase as the SDS concentrations increase in the system (**Figure**
18 **6 (c)**). The nanoparticles' density peaks at water-heptane interfaces are shifted from 8.7 nm to 7.6
19 nm as the SDS concentration increased from 0 wt.% to 0.1 wt.%, respectively. Similarly, the
20 density peaks of nanoparticles are shifted from 8.5 nm to 8.3 nm as the SDS concentrations
21 increased from 0 wt.% to 0.1 wt.%, respectively. The shift toward the aqueous phase suggests that
22 the assembled SDS molecules on the interfaces displace the assembled nanoparticles away from

1 the interface. This observation is consistent with the USAXS/SAXS intensities (**Figure 2 and 3**)
2 and agrees with previous studies.²⁹

3 The displacement of nanoparticles from the interface is also evident from the density of
4 water molecules around the surface of nanoparticles. These densities are quantified by calculating
5 the radial distribution function ($g(r)$) of oxygen atoms in water molecules from the hydroxyl
6 groups (-OH) on the surface of silica nanoparticles as a reference atom (**see Figure 7**). The peaks
7 represent the first coordination shells and second coordination shells of the oxygen in the water
8 molecule around silica -OH groups. The density of the first and second coordination shells
9 increased systematically with the increase in SDS concentrations. The denser water shells stem
10 from the exposure of nanoparticle surface to water molecules that cover the nanoparticle as it is
11 displaced from the interface and emerges into the aqueous phase to solvate the surfaces of
12 nanoparticles and reduce its surface free energy.

13 **3.2. Interfacial properties**

14 The influence of SDS surfactants on the assembly of silica nanoparticles and the resulting
15 impact on the interfacial properties of water-heptane and water-toluene emulsions is probed from
16 the MD simulation trajectories. Water-heptane and water-toluene formed two distinct phases with
17 average densities of about 994, 658 and 862 kg/m³ for water, heptane, and toluene phases,
18 respectively (**see Figure 6**), which is in excellent agreement with the experimental bulk and
19 emulsion densities at the conditions of 1 bar and 298 K.^{67, 68} The influence of silica nanoparticles
20 and SDS surfactants on the interfacial properties is quantified by calculating the interfacial tensions
21 of the studied emulsions (**Figure 8**) as follow:^{69, 70}

$$\gamma_{WH} = \frac{1}{n} \left(P_{zz} - \frac{P_{xx} + P_{yy}}{2} \right) L_z \quad (2)$$

In this expression, γ_{WH} is the interfacial tension of water-heptane and water-toluene mixtures, n is the number of interfaces in the simulation cell, P_{ii} is the pressure (where $i = x, y$ and z directions) and L_z is the equilibrium cell length in the direction normal to the interface (z direction).

The calculated interfacial tensions of water-heptane and water-toluene at 1 bar and 298 K are 51.8 mN/m and 36.4 mN/m, respectively, which are consistent with prior experimental and simulation results.^{67, 71} Introducing silica nanoparticles to the interface resulted in a 4.7 % and 9.4 % reduction in the interfacial tension of water-heptane and water-toluene mixtures, respectively. Increases in the SDS concentrations to 0.01 wt% resulted in a slight reduction in the interfacial tension of both emulsions due to the addition of limited quantities of surfactant molecules that accumulate at the water-hydrocarbon interfaces. A substantial reduction in the interfacial tensions of both emulsions is observed on adding 0.1 wt.% of SDS to the systems. The interfacial tension of water-heptane and water-toluene decreased to 24.3 and 9.1 mN/m, respectively. These results suggest that high concentrations of SDS are more effective in stabilizing the emulsion of interest compared to hydrophilic silica nanoparticles. The simulations and experiments reveal that the stabilization of water-hydrocarbon emulsions in the presence of high concentrations of SDS surfactants is accompanied by limiting the assembly of silica nanoparticles at water-hydrocarbon interfaces.

The mechanism by which silica nanoparticles and SDS molecules reduce the interfacial tension of water-heptane and water-toluene emulsions involves the assembly and dispersion of these nanoparticles and surfactants at the interface (see **Figure 9**). Silica nanoparticles form a

1 cluster of five nanoparticles at water-heptane and water-toluene in the absence of SDS molecules.
2 Interestingly, the aggregation number of the nanoparticles decreases systematically as the SDS
3 concentration increases (**Figure 9 A and B**) due to the preferential assembly of the SDS molecules
4 at the interfacial region (**Figure 9 C and D**). Thus, the reduction in the interfacial tensions is driven
5 by three scenarios (**Figure 9 E**): (a) the presence of nanoparticles at the interface results in slight
6 reduction in the interfacial tension, (b) the coexistence of nanoparticles and surfactants at the
7 interface results in a greater reduction in the interfacial scenario compared to the first scenario,
8 and (c) the excess SDS molecules at the interfaces of water-heptane and water-toluene reduces the
9 interfacial tension significantly.

10 **3.3. Energetics associated with the assembly of silica nanoparticles and SDS surfactants**

11 The intermolecular interactions of silica nanoparticles with water and hydrocarbons are
12 probed to elucidate the energetic basis underlying their observed assembly as a function of SDS
13 concentration (**see Figure 10**). The van der Waals and electrostatic interactions averaged over the
14 last 10 ns of the simulation constitute the intermolecular interactions of interest. The
15 intermolecular interactions of the nanoparticles with water molecules are higher than the
16 interactions of nanoparticles with heptane and toluene due to the hydrophilic nature of silica
17 nanoparticles that drives the largest portion of the interfacial nanoparticle surface to be covered by
18 water molecules.

19 Interestingly, the interactions of nanoparticles with water in water-heptane and water-
20 toluene systems increase systematically with the SDS concentrations. The increase in
21 nanoparticles-water interactions is associated with a systematic decrease in the magnitude of
22 nanoparticle-heptane and nanoparticle-toluene interaction energies. The trends of nanoparticles-

1 water and nanoparticles-hydrocarbons energetic interactions as SDS concentrations increase
2 confirms the displacement of nanoparticles from the interfaces to the aqueous phase by SDS
3 molecules. The displacement of the nanoparticles toward the aqueous phase is also confirmed by
4 the increase of the average number of water molecules in the first coordination shell of the
5 hydroxyl group on the surface of the nanoparticles (**see Table 1**). The number of O_{water} in the first
6 coordination shell of $\text{OH}_{\text{silica}}$ increases systematically with the increase of SDS concentrations in
7 the hydrocarbon phases, indicating the increase of water density around the displaced
8 nanoparticles. The enhanced solvation of silica nanoparticles due to the displacement into the
9 aqueous phase is associated with an increase in the number of the hydrogen bonds between the
10 hydroxyl groups on the surface of the nanoparticles and the surrounding water molecules (**see**
11 **Figure S4**).

12 Van der Waals interactions contribute significantly to the coexistence of silica
13 nanoparticles and SDS surfactant at the interfaces of water-heptane and water-toluene emulsions,
14 with electrostatic interactions having minor contribution (**see Table 2**). Van der Waals and
15 electrostatic interactions increase systematically with the concentrations of SDS due to the
16 assembly of SDS at the interfaces. Further, Van der Waals and electrostatic interactions between
17 the interfacial nanoparticles and surfactants are higher at water-toluene compared to at water-
18 heptane at all SDS concentrations. The higher intermolecular interactions of nanoparticles-SDS at
19 the interface of water-toluene explains the significant reduction in the interfacial tension driven by
20 the synergetic interactions between the interfacial nanoparticles and surfactants. However, the
21 increase in the hydrogen binding of nanoparticles-water (**Figure S4**) and SDS-water (**Figure S5**)
22 with the increase of SDS concentrations confirms the favorable adsorption of SDS surfactant at
23 the interface over the silica nanoparticles.

1 Interestingly, attractive electrostatic interactions of nanoparticles with water are noted
2 while the van der Waals interactions between the OH-terminated nanoparticles and water
3 molecules are repulsive (**see Table 3**). Hydrogen bonding between the hydroxyl groups on the
4 nanoparticles surfaces and water molecules contributed positively to the strong attraction between
5 the nanoparticles and the aqueous phase. Nanoparticle interactions with heptane are dominated by
6 van der Waals interactions with minor contributions of coulomb attraction, while the interaction
7 with toluene includes a substantial contribution from van der Waals and electrostatic interactions.
8 The interaction energies elucidate the systematic displacement of silica nanoparticles from water-
9 heptane and water-toluene interfaces that observed from USAXS/SAXS measurements, cryo-SEM
10 imaging and MD simulations.

11 **4. Conclusions**

12 In this study, we uncover the mechanisms underlying the stabilization of water-toluene and
13 water-heptane emulsions in the presence of silica nanoparticles with diameters of 50 nm and 100
14 nm and surfactant concentrations ranging from 0.001 wt% to 0.1 wt%. At low SDS concentrations
15 of 0 wt% and 0.001%, emulsion stabilization proceeds via the assembly of silica nanoparticles at
16 water-hydrocarbon interfaces. However, at higher SDS concentrations of 0.1%, emulsion
17 stabilization occurs via the assembly of surfactants at the water-hydrocarbon interface and the
18 associated displacement of silica nanoparticles away from this interface. The interfacial tensions
19 and the energetics calculated from the simulations underlying these emulsion stabilization
20 mechanisms support experimental observations of the differences in the assembly of silica
21 nanoparticles and surfactants at the water-hydrocarbon interface. The reduction in the interfacial
22 tensions occurs solely due to the assembly of silica nanoparticles at the interfaces in the presence
23 of low SDS concentrations. However, the interfacial tensions reduce significantly in the presence

1 of 0.1% SDS because of the assembly of surfactants that displace the interfacial nanoparticles
2 toward the aqueous phase. These insights provide the physico-chemical basis for designing energy-
3 efficient water and hydrocarbon separations to advance sustainable energy and environmental
4 technologies. Further experimental and computational studies are needed to resolve the effect of
5 the surface curvature of silica nanoparticles and their solutions' pH values on their interfacial
6 behavior at immiscible liquids interfaces.

7 **Acknowledgment**

8 This work was supported as part of the Multi-Scale Fluid-Solid Interactions in Architected and
9 Natural Materials (MUSE), an Energy Frontier Research Center funded by the U.S. Department
10 of Energy, Office of Science, Basic Energy Sciences under Award # DE-SC0019285. The use of
11 the Advanced Photon Source, an Office of the Science User Facility operated for the U.S.
12 Department of Energy (DOE) Office of Science by Argonne National Laboratory, is supported by
13 the U.S. DOE under Contract DE-AC02-06CH11357. The authors would also like to acknowledge
14 Dr. Katie Spoth who helped in taking the Cryogenic SEM images using Cornell Center for
15 Materials Research shared facilities which supported through the NSF MRSEC program (DMR-
16 1719875).

17 **References**

- 18 1. N. Yekeen, E. Padmanabhan, A.K. Idris and S.M. Ibad, *J. Petrol. Sci. Eng.*, 2019, **179**.
- 19 2. C. Omurlu, H. Pham and Q.P. Nguyen, *Appl. Nanosci.*, 2016, **6**, 1167-1173.
- 20 3. S. Rahman, J.J. Tamborski, M.A. Charette and J.K. Cochran, *Mar. Chem.*, 2019, **208**, 29-
21 42.
- 22 4. J. Faria, M.P. Ruiz and D.E. Resasco, *Adv. Synth. Catal.*, 2010, **352**, 2359-2364.

- 1 5. L. Leclercq, A. Mouret, A. Proust, V. Schmitt, P. Bauduin, J.M. Aubry and V.
2 Nardello-Rataj, *Chem. A Euro. J.*, 2012, **18**, 14352-14358.
- 3 6. F. Tang, L. Li and D. Chen, *Adv. Mater.*, 2012, **24**, 1504-1534.
- 4 7. M. Manzano and M. Vallet-Regí, *Adv. Funct. Mater.*, 2020, **30**, 1902634.
- 5 8. Z. H. Zhou, J. Wang, X. Liu and H.S.O. Chan, *J. Mater. Chem.*, 2001, **11**, 1704-1709.
- 6 9. E. B. Mock, H. De Bruyn, B.S. Hawkett, R.G. Gilbert and C.F. Zukoski, *Langmuir*, 2006,
7 **22**, 4037-4043.
- 8 10. P. Shinde, S.S. Gupta, B. Singh, V. Polshettiwar and B.L. Prasad, *J. Mater. Chem. A*, 2017,
9 **5**, 14914-14921.
- 10 11. S. Hasebe, S. Aoyama, M. Tanaka and H. Kawakami, *J. Membr. Sci.*, 2017, **536**, 148-155.
- 11 12. A. Burns, P. Sengupta, T. Zedayko, B. Baird and U. Wiesner, *Small*, 2006, **2**, 723-726.
- 12 13. M. Lundqvist, I. Sethson and B.H. Jonsson, *Langmuir*, 2004, **20**, 10639-10647.
- 13 14. S. J. D. Sofla, L.A. James and Y. Zhang, *Fuel*, 2018, **216**, 559-571.
- 14 15. E. Dickinson, *Trends Food Sci. Tech.*, 2012, **24**, 4-12.
- 15 16. K. Zhang, Q. Wang, H. Meng, M. Wang, W. Wu and J. Chen, *Particuology*, 2014, **14**, 12-
16 18.
- 17 17. R. Pichot, F. Spyropoulos and I.T. Norton, *J. Colloid Interf. Sci.*, 2012, **377**, 396-405.
- 18 18. T. V. Vu and D.V. Papavassiliou, *J. Colloid Interf. Sci.*, 2019, **553**, 50-58.
- 19 19. H. Ma, M. Luo and L.L. Dai, *Phys. Chem. Chem. Phys.*, 2008, **10**, 2207-2213.
- 20 20. N. G. Eskandar, S. Simovic and C.A. Prestidge, *Phys. Chem. Chem. Phys.*, 2007, **9**, 6426-
21 6434.
- 22 21. A. J. Worthen, L.M. Foster, J. Dong, J.A. Bollinger, A.H. Peterman, L.E. Pastora, S.L.
23 Bryant, T.M. Truskett, C.W. Bielawski and K.P. Johnston, *Langmuir*, 2014, **30**, 984-994.

- 1 22. R. U. Ranatunga, C.T. Nguyen, B.A. Wilson, W. Shinoda and S.O. Nielsen, *Soft Matter*,
2 2011, **7**, 6942-6952.
- 3 23. B. P. Binks and J.A. Rodrigues, *Langmuir*, 2007, **23**, 7436-7439.
- 4 24. I. Akartuna, A.R. Studart, E. Tervoort, U.T. Gonzenbach and L.J. Gauckler, *Langmuir*,
5 2008, **24**, 7161-7168.
- 6 25. B. P. Binks and C.P. Whitby, *Colloid. Surface. A*, 2005, **253**, 105-115.
- 7 26. W. Wang, Z. Zhou, K. Nandakumar, Z. Xu and J.H. Masliyah, *J. Colloid Interf. Sci.*, 2004,
8 **274**, 625-630.
- 9 27. N. R. Biswal, N. Rangera and J.K. Singh, *J. Phys. Chem. B*, 2016, **120**, 7265-7274.
- 10 28. R. Pichot, F. Spyropoulos and I.T. Norton, *J. Colloid Interf. Sci.*, 2010, **352**, 128-135.
- 11 29. C. Vashisth, C.P. Whitby, D. Fornasiero and J. Ralston, *J. Colloid Interf. Sci.*, 2010, **349**,
12 537-543.
- 13 30. S. Levine, B.D. Bowen and S.J. Partridge, *Colloid. Surface.*, 1989, **38**, 325-343.
- 14 31. D. E. Tambe and M.M. Sharma, *J. Colloid Interf. Sci.*, 1993, **157**, 244-253.
- 15 32. J. H. Schulman and J. Leja, *T. Faraday Soc.*, 1954, **50**, 598-605.
- 16 33. E. H. Lucassen-Reynders and M.V.D. Tempel, *J. Phys. Chem.*, 1963, **67**, 731-734.
- 17 34. H. Hassander, B. Johansson and B. Törnell, *Colloid. Surface.*, 1989, **40**, 93-105.
- 18 35. F. Ravera, E. Santini, G. Loglio, M. Ferrari and L. Liggieri, *J. Phys. Chem. B*, 2006, **110**,
19 19543-19551.
- 20 36. J. Wang, F. Yang, C. Li, S. Liu and D. Sun, *Langmuir*, 2008, **24**, 10054-10061.
- 21 37. S. Mohammed, H. Asgar, I. Kuzmenko and G. Gadikota, *Energy Fuels*, 2020, **34**, 12545–
22 12555.

- 1 38. J. Ilavsky, P.R. Jemian, A.J. Allen, F. Zhang, L.E. Levine, G.G. Long, *J. Appl. Crystallogr.*,
2 2009, **42**, 469-479.
- 3 39. J. Ilavsky, F. Zhang, A.J. Allen, L.E. Levine, P.R. Jemian and G.G. Long, *Metall. Mater.*
4 *Trans. A*, 2013, **44**, 68-76.
- 5 40. J. Ilavsky, *J. Appl. Crystallogr.*, 2012, **45**, 324-328.
- 6 41. J. Ilavsky and P.R. Jemian, *J. Appl. Crystallogr.*, 2009, **42**, 347-353.
- 7 42. G. Yu and J. Zhou, *Phys. Chem. Chem. Phys.*, 2016, **18**, 23500-23507.
- 8 43. D. Argyris, N.R. Tummala, A. Striolo and D.R. Cole, *J. Phys. Chem. C*, 2008, **112**, 13587-
9 13599.
- 10 44. D. Argyris, D.R. Cole and A. Striolo, *Langmuir*, 2009, **25**, 8025-8035.
- 11 45. A. Phan, D.R. Cole and A. Striolo, *J. Phys. Chem. C*, 2014, **118**, 4860-4868.
- 12 46. R. T. Cygan, J.J. Liang and A.G. Kalinichev, *J. Phys. Chem. B*, 2004, **108**, 1255-1266.
- 13 47. W. L. Jorgensen, J.D. Madura and C.J. Swenson, *J. Am. Chem. Soc.*, 1984, **106**, 6638-
14 6646.
- 15 48. W. L. Jorgensen, D.S. Maxwell and J. Tirado-Rives, *J. Am. Chem. Soc.*, 1996, **118**, 11225-
16 11236.
- 17 49. V. S. Farafonov and A.V., Lebed, *J. Chem. Theory Comput.*, 2017, **13**, 2742-2750.
- 18 50. T. Fang, Y. Zhang, R. Ma, Y. Yan, C. Dai and J. Zhang, *Appl. Surf. Sci.*, 2019, **494**, 80-86.
- 19 51. B. Meghwal, N. Rampal and A. Malani, *Energy Fuels*, 2020, **34**, 16023-16034.
- 20 52. H. Yan and S. Yuan, *J. Phys. Chem. C*, 2016, **120**, 2667-2674.
- 21 53. S. Nosé, *Mol. Phys.*, 1984, **52**, 255-268.
- 22 54. W. G. Hoover, *Phys. Rev. A*, 1985, **31**, 1695.
- 23 55. M. Parrinello and A. Rahman, *J. Chem. Phys.*, 1982, **76**, 2662-2666.

- 1 56. T. Darden, D. York and L. Pedersen, *J. Chem. Phys.*, 1993, **98**, 10089–10092.
- 2 57. M. J. Abraham, T. Murtola, R. Schulz, S. Páll, J.C. Smith, B. Hess and E. Lindahl,
3 *SoftwareX*, 2015, **1**, 19-25.
- 4 58. Y. Chai, J. Hasnain, K. Bahl, M. Wong, D. Li, P. Geissler, P.Y. Kim, Y. Jiang, P. Gu, S.
5 Li and D. Lei, *Sci. Adv.*, 2020, **6**, eabb8675.
- 6 59. M. Zargartalebi, N. Barati and R. Kharrat, *J. Petrol. Sci. Eng.*, 2014, **119**, 36-43.
- 7 60. T. Li, A.J. Senesi and B. Lee, *Chem. Rev.*, 2016, **116**, 11128-11180.
- 8 61. A. Czajka and S.P. Armes, *J. Am. Chem. Soc.*, 2021, **143**, 1474-1484.
- 9 62. S. Svenson, *Curr. Opin. Colloid In. Sci.*, 2004, **9**, 201-212.
- 10 63. W. Shinoda, R. DeVane and M.L. Klein, *Soft Matter*, 2008, **4**, 2454-2462.
- 11 64. W. X. Shi and H.X. Guo, *J. Phys. Chem. B*, 2010, **114**, 6365-6376.
- 12 65. P. W. Schmidt, *J. Appl. Crystallogr.*, 1991, **24**, 414-435.
- 13 66. J. Teixeira, *J. Appl. Crystallogr.*, 1988, **21**, 781-785.
- 14 67. T. Lan, H. Zeng and T. Tang, *J. Phys. Chem. C*, 2019, **123**, 22989-22999.
- 15 68. X. Sun, H. Zeng and T. Tang, *J. Colloid Interface Sci.*, 2021, **586**, 766-777.
- 16 69. S. Mohammed and G.A., Mansoori, *Energy Fuels*, 2018, **32**, 5409-5417.
- 17 70. S. Mohammed and G.A., Mansoori, *J. Mol. Liq.*, 2018, **263**, 268-273.
- 18 71. A. H. S. Dehaghani, M.S. Taleghani, M.H. Badizad and R. Daneshfar, *Colloid Interf. Sci.*
19 *Commun.*, 2019, **33**, 100202.
- 20
- 21
- 22

1 **Table 1.** The number of water oxygens in the first coordination shell of hydroxyl group on the
2 silica nanoparticles surface as a function of SDS concentrations. The data are averaged over the
3 last 10 ns of the simulation time and the error bars represent the standard deviation from the mean
4 value of three different simulations.

SDS concentration (wt%)	Water-heptane	Water-toluene
0	0.43 ± 0.01	0.43 ± 0.02
0.001	0.45 ± 0.04	0.44 ± 0.01
0.01	0.47 ± 0.02	0.47 ± 0.03
0.1	0.48 ± 0.02	0.54 ± 0.01

5
6
7
8
9
10
11
12
13
14
15
16
17
18
19
20
21
22
23
24
25
26

1 **Table 2.** Van der Waals and electrostatic interactions (kJ/mol) of silica nanoparticles with SDS
2 surfactant at the interfaces of water-heptane and water-toluene as a function of SDS
3 concentrations. The data are averaged over the last 10 ns of the simulation time and the error bars
4 represent the standard deviation from the mean value of three different simulations.

SDS concentration (wt%)	Water-heptane interface		Water-toluene interface	
	van der Waals	Electrostatic	van der Waals	Electrostatic
0.001	-2.52 ± 0.04	-0.43 ± 0.02	-2.60 ± 0.01	-0.45 ± 0.04
0.01	-16.10 ± 0.12	-2.41 ± 0.08	-23.05 ± 0.27	-3.35 ± 0.09
0.1	-43.25 ± 1.39	-5.19 ± 0.42	-69.207 ± 2.03	-11.02 ± 0.21

5
6
7
8
9
10
11
12
13
14
15
16
17
18
19
20
21
22
23
24
25
26
27

1 **Table 3.** Van der Waals and electrostatic interactions of silica nanoparticles with water, heptane
 2 and toluene phases (kJ/mol) as a function of SDS concentrations. The data are averaged over the
 3 last 10 ns of the simulation time and the error bars represent the standard deviation from the mean
 4 value of three different simulations.

SDS concentration (wt. %)	silica nanoparticles- water interactions		silica nanoparticles- hydrocarbon interactions	
	Van der Waals	Electrostatic	Van der Waals	Electrostatic
Water-heptane				
0	1435.4 ± 11	-18805.4 ± 49	-1150.67 ± 11	-45.46 ± 5
0.001	1461.8 ± 12	-20155.9 ± 48	-874.658 ± 16	-33.65 ± 4
0.01	1489.8 ± 19	-20495.0 ± 31	-748.29 ± 8	-26.18 ± 1
0.1	1499.3 ± 20	-20545.6 ± 19	-634.7 ± 12	-22.14 ± 2
Water-toluene				
0	1378.1 ± 10	-19614.7 ± 53	-884.7 ± 14	-970.2 ± 12
0.001	1454.0 ± 23	-20135.9 ± 49	-774.7 ± 18	-953.4 ± 11
0.01	1476.7 ± 23	-20224.0 ± 51	-648.3 ± 13	-951.1 ± 13
0.1	1527.3 ± 16	-21426.6 ± 21	-534.7 ± 9	-353.4 ± 6

5
6
7
8
9
10
11
12
13
14
15
16
17
18
19
20
21

1 Captions for figures

2 **Figure 1.** Schematic representation of the experimental setup of ultra-small/small-angle X-ray scattering
3 (USAXS/SAXS) measurements of silica nanoparticles and sodium dodecyl sulfate surfactant at water-
4 heptane and water-toluene interfaces is shown in panel (a). Snapshots of the simulated initial configuration
5 of the suspended silica nanoparticle in the water phase and the suspended SDS molecules in the hydrocarbon
6 phase is shown in panel (b). The atoms of silica nanoparticles (see the color coding for the atoms) and SDS
7 molecules are drawn using VDW drawing method while water and hydrocarbons molecules are drawn using
8 Lines method implemented in VMD visualization software.

9 **Figure 2.** Combined USAXS/SAXS data scattered from water-heptane and water-toluene interfaces in the
10 presence of (a) 50 nm nanoparticles on water-heptane, (b) 50 nm nanoparticles on water-toluene, (c) 100
11 nm nanoparticles on water-heptane and (d) 100 nm nanoparticles on water-toluene interfaces as a function
12 of the SDS concentrations.

13 **Figure 3.** Number of (a) 50 nm nanoparticles at water-heptane, (b) 50 nm nanoparticles at water-toluene,
14 (c) 100 nm nanoparticles at water-heptane and (d) 100 nm nanoparticles at water-toluene interfaces as a
15 function of SDS concentrations. The x-axis represents the size distribution of the interfacial silica
16 nanoparticles. These data are governed from modeling the USAXS/SAXS scattering curves.

17 **Figure 4.** Power law slope of the scattering curves in the ultrasmall angle X-ray scattering region of water-
18 heptane and water-toluene emulsions with 50 nm and 100 nm silica nanoparticles as a function of SDS
19 concentrations.

20 **Figure 5.** Cryogenic scanning electron microscopy images of water-heptane and water-toluene interfaces
21 in the presence of 0.001 wt.% and 0.1 wt.% SDS concentrations. The images are taken from systems
22 containing 100 nm silica nanoparticles.

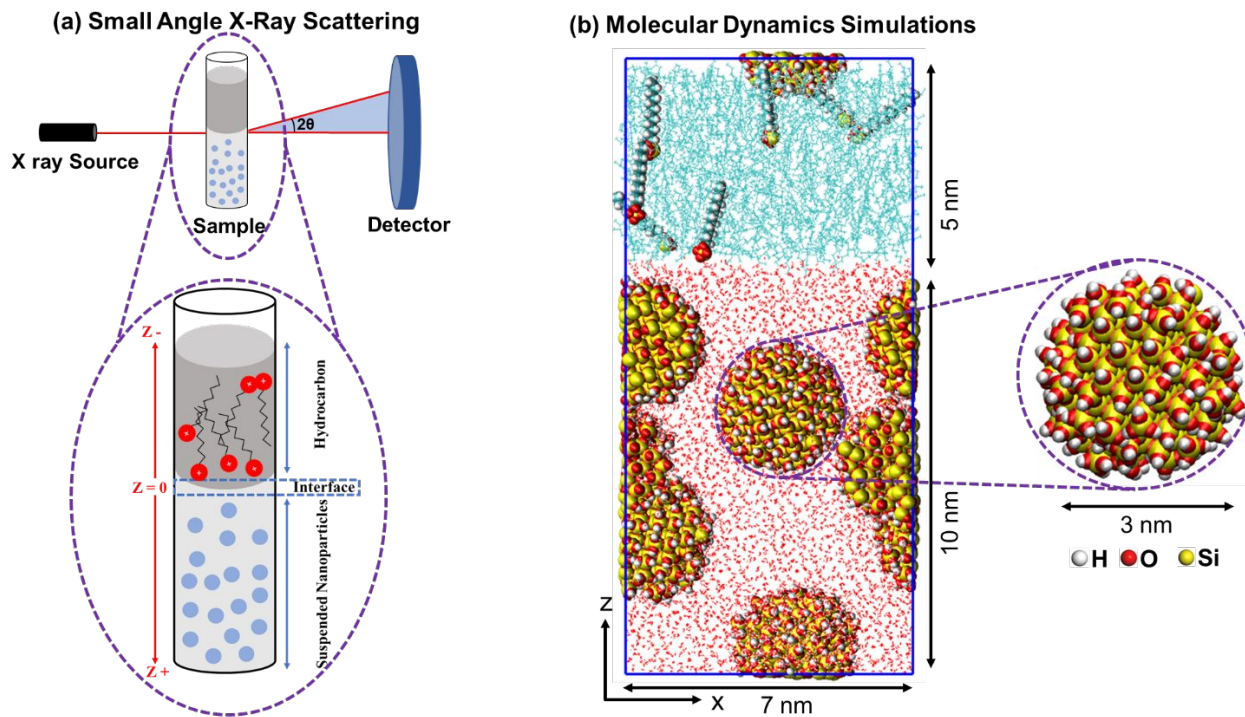
23 **Figure 6.** The density profiles along the axis normal to the interface (z-axis) of (a) water-heptane system
24 constituents in the presence of 0.1 wt.% SDS, (b) water-toluene system constituents in the presence of 0.1
25 wt.% SDS, (c) nanoparticles in water-heptane system as a function of SDS concentrations and (d)
26 nanoparticles in water-toluene as a function of SDS concentrations. The density profiles are averaged over
27 the last 10 ns of the simulation time.

28 **Figure 7.** The radial distribution function of oxygen atoms in water molecules from -OH groups on the
29 silica nanoparticles surfaces as a function of SDS concentrations. The radial distribution functions are
30 averaged over the last 10 ns of the simulation time.

31 **Figure 8.** The interfacial tension of water-heptane and water-toluene emulsions in the absence and presence
32 of silica nanoparticles as a function of SDS concentrations. The interfacial tensions are averaged over the
33 last 10 ns of the simulation time. The error bars represent the standard deviation from the mean value of
34 three different simulations.

35 **Figure 9.** The aggregation number of silica nanoparticles in (A) water-heptane and (B) water-toluene
36 emulsions as a function of the SDS concentration. The assembly of SDS molecules at (C) water-heptane
37 and (D) water-toluene interfaces are characterized by calculating the average aggregation number of SDS
38 molecules at a concentration of 0.01 and 0.1 wt%. (E) Schematics show the interfacial configurations of
39 silica nanoparticles and SDS surfactant at water-hydrocarbons interfaces at different SDS concentrations.

40 **Figure 10.** The intermolecular interaction of nanoparticles with (a) water and heptane in water-heptane
41 emulsion and (b) water and toluene in water-toluene emulsion as a function of the SDS concentrations. The
42 intermolecular interactions are averaged over the last 10 ns of the simulation time. The error bars represent
43 the standard deviation from the mean value of three different simulations.



1

2

3 **Figure 1.** Schematic representation of the experimental setup of ultra-small/small-angle X-ray
 4 scattering (USAXS/SAXS) measurements of silica nanoparticles and sodium dodecyl sulfate
 5 surfactant at water-heptane and water-toluene interfaces is shown in panel (a). Snapshot of the
 6 simulated initial configuration of the suspended silica nanoparticle in the water phase and the
 7 suspended SDS molecules in the hydrocarbon phase is shown in panel (b). The atoms of silica
 8 nanoparticles (see the color coding for the atoms) and SDS molecules are drawn using VDW
 9 drawing method while water and hydrocarbons molecules are drawn using Lines method
 10 implemented in VMD visualization software.

11

12

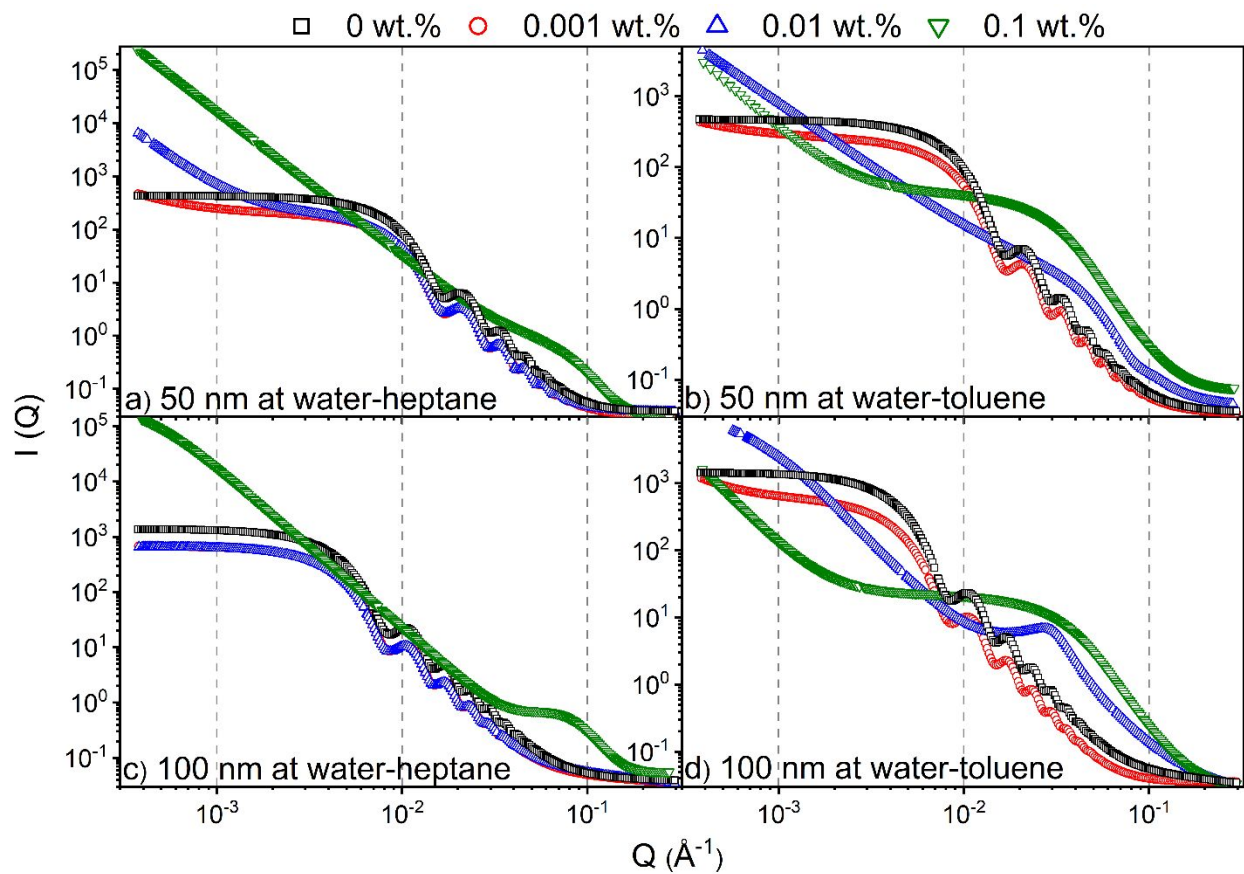
13

14

15

16

17



1

2 **Figure 2.** Combined USAXS/SAXS scattering curves from water-heptane and water-toluene
 3 interfaces in the presence of **(a)** 50 nm nanoparticles on water-heptane, **(b)** 50 nm nanoparticles
 4 on water-toluene, **(c)** 100 nm nanoparticles on water-heptane and **(d)** 100 nm nanoparticles on
 5 water-toluene interfaces as a function of the SDS concentrations.

6

7

8

9

10

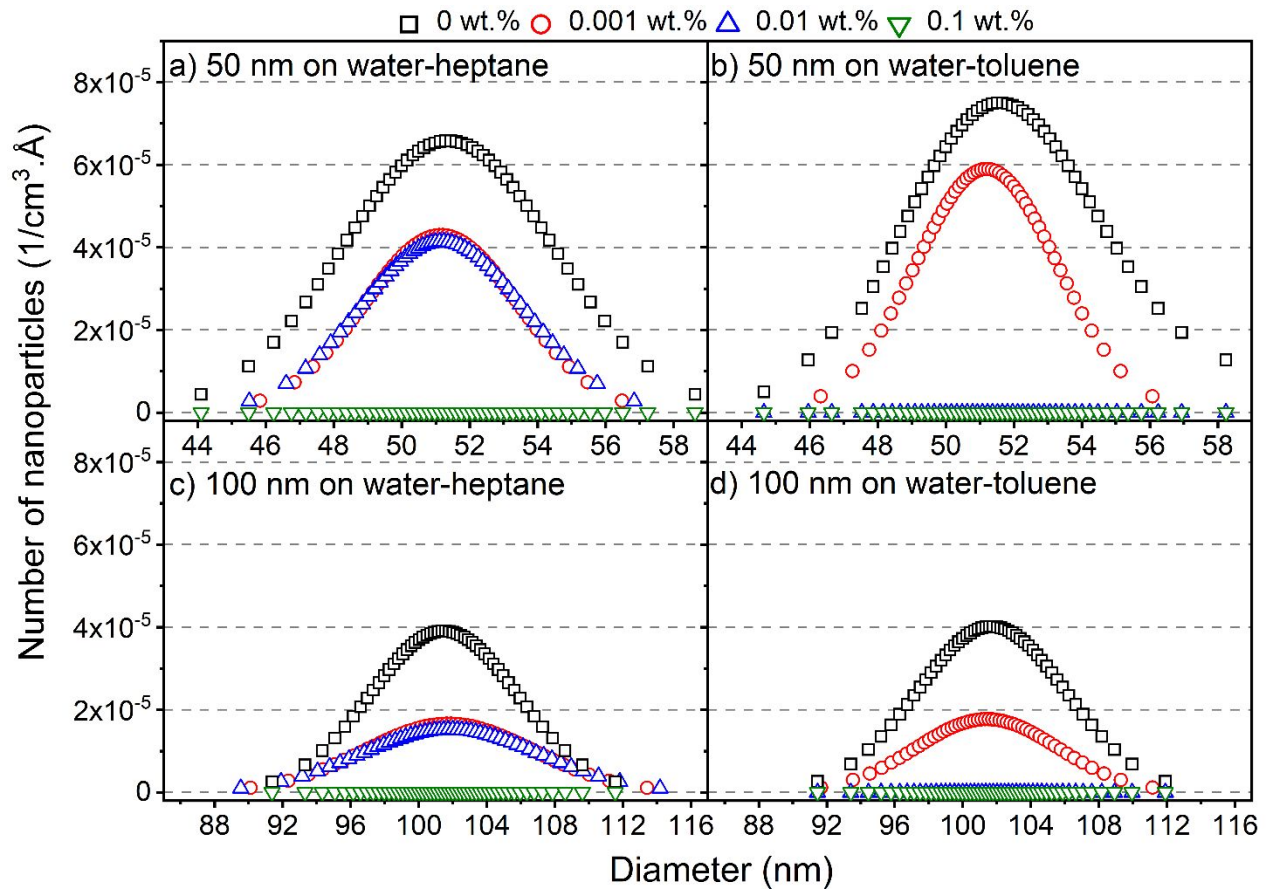
11

12

13

14

15



1

2 **Figure 3.** Number of (a) 50 nm nanoparticles at water-heptane, (b) 50 nm nanoparticles at water-
 3 toluene, (c) 100 nm nanoparticles at water-heptane and (d) 100 nm nanoparticles at water-toluene
 4 interfaces as a function of SDS concentrations. The x-axis represents the size distribution of the
 5 interfacial silica nanoparticles. These data are governed from modeling the USAXS/SAXS
 6 scattering curves.

7

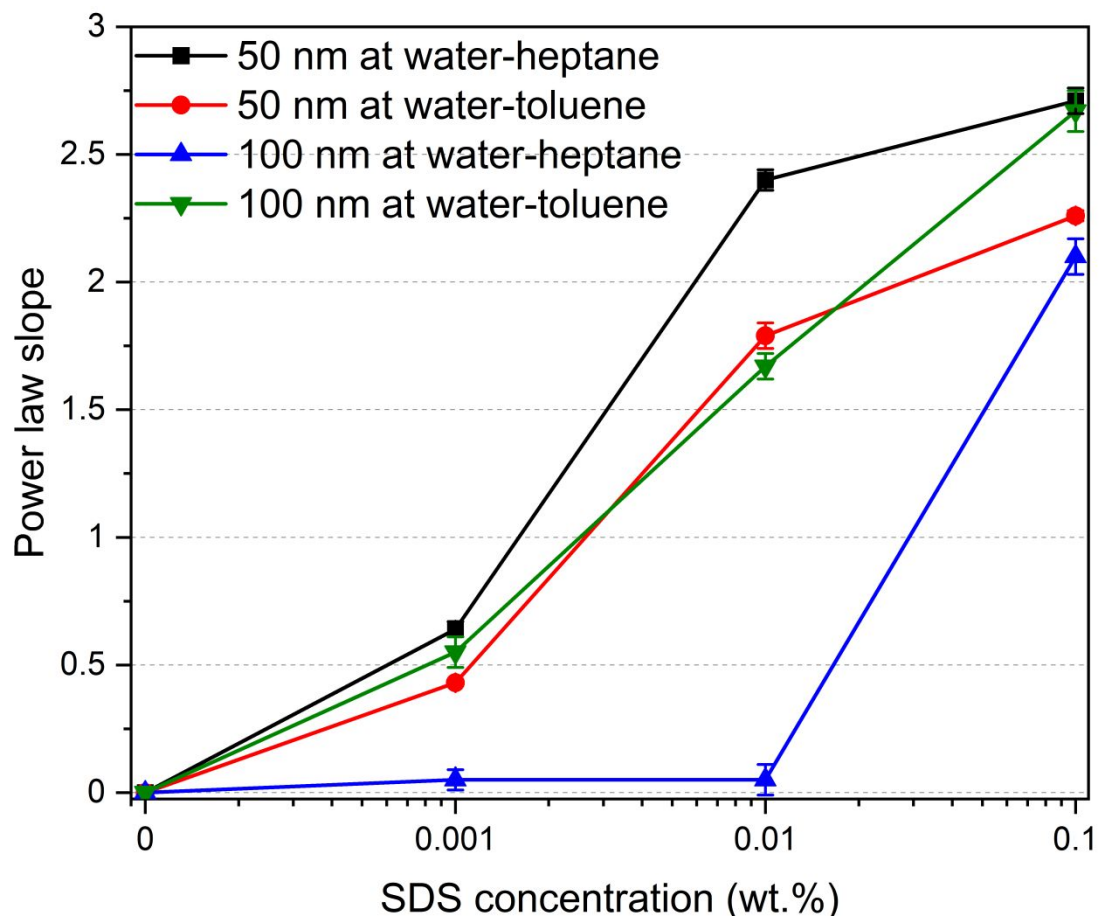
8

9

10

11

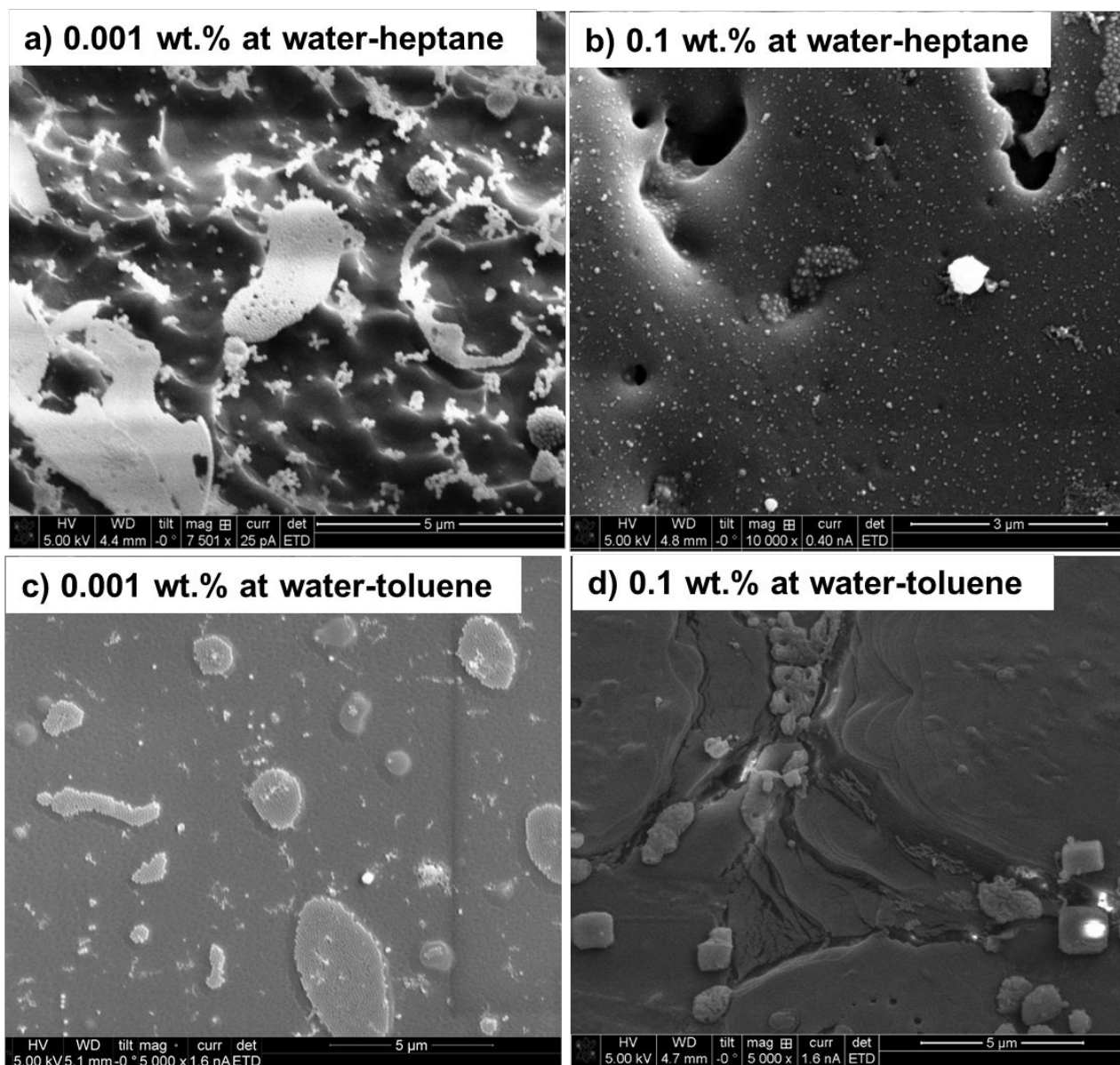
12



1

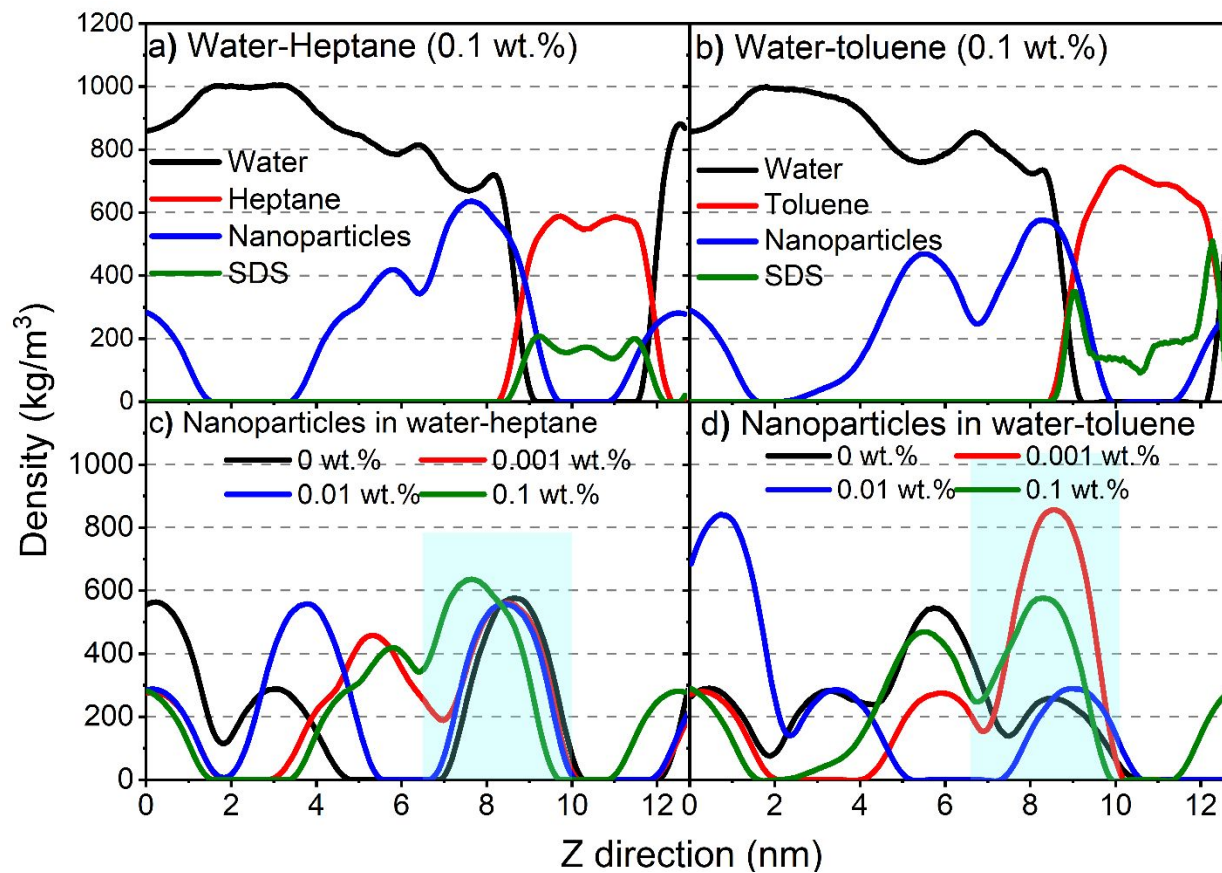
2 **Figure 4.** Power law slope of the scattering curves in the ultrasmall angle X-ray scattering region
3 of water-heptane and water-toluene emulsions with 50 nm and 100 nm silica nanoparticles as a
4 function of SDS concentrations.

5



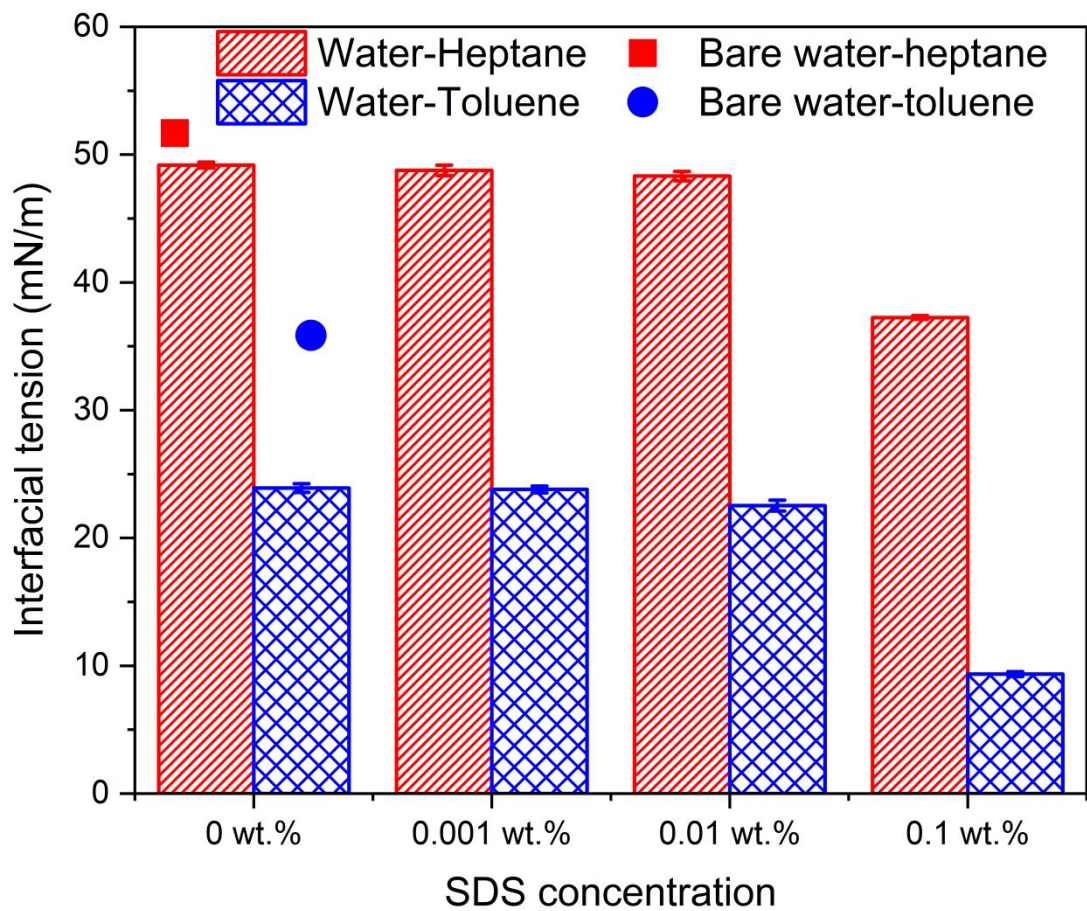
1
2 **Figure 5.** Cryogenic scanning electron microscopy images of water-heptane and water-toluene
3 interfaces in the presence of 0.001 wt.% and 0.1 wt.% SDS concentrations. The images are taken
4 from systems containing 100 nm silica nanoparticles.

5
6
7



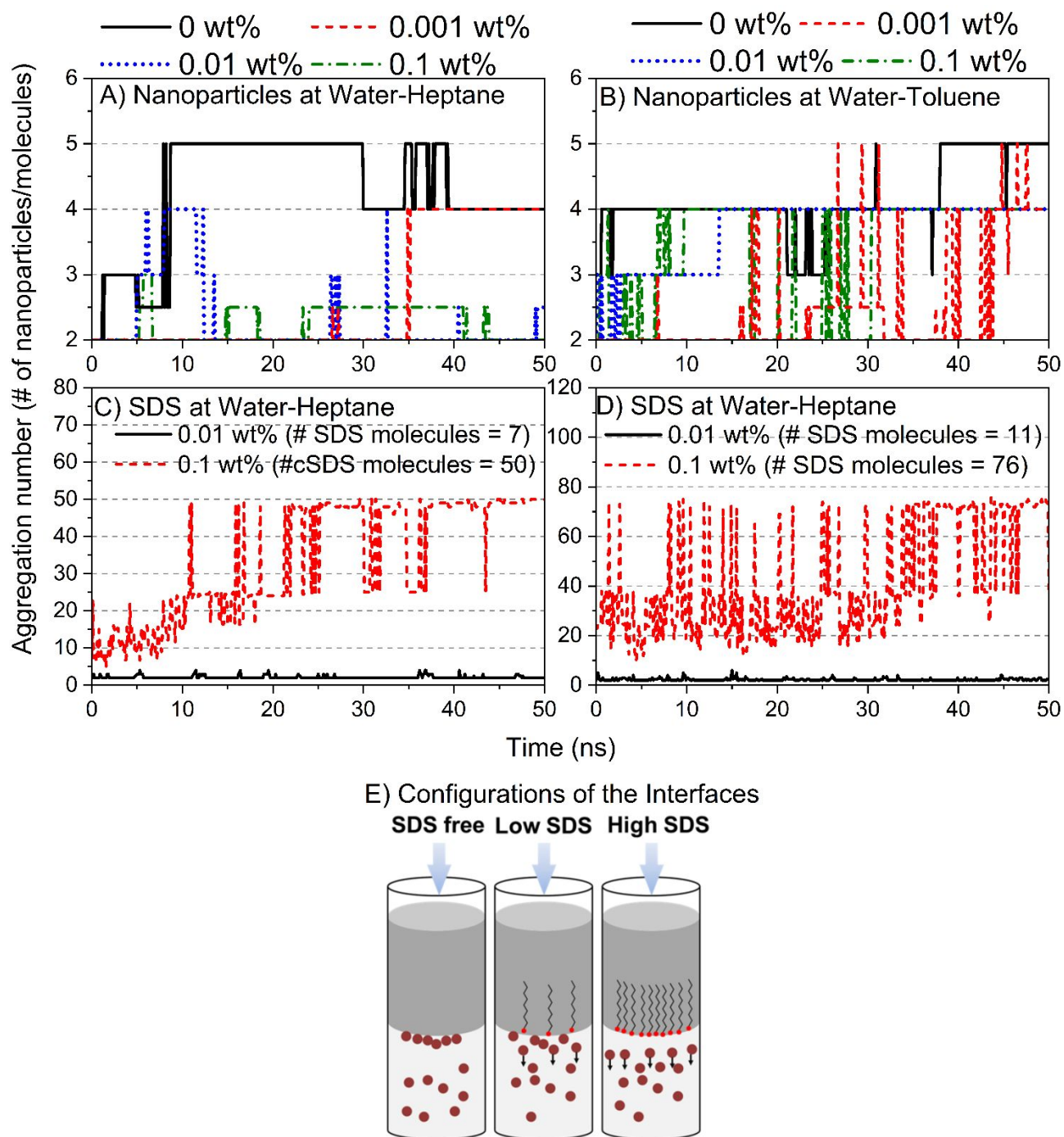
1
 2 **Figure 6.** The density profiles along the axis normal to the interface (z-axis) of (a) water-heptane
 3 system constituents in the presence of 0.1 wt.% SDS, (b) water-toluene system constituents in the
 4 presence of 0.1 wt.% SDS, (c) nanoparticles in water-heptane system as a function of SDS
 5 concentrations and (d) nanoparticles in water-toluene as a function of SDS concentrations. The
 6 density profiles are averaged over the last 10 ns of the simulation time.

7



1
2
3
4
5
6
7
8
9

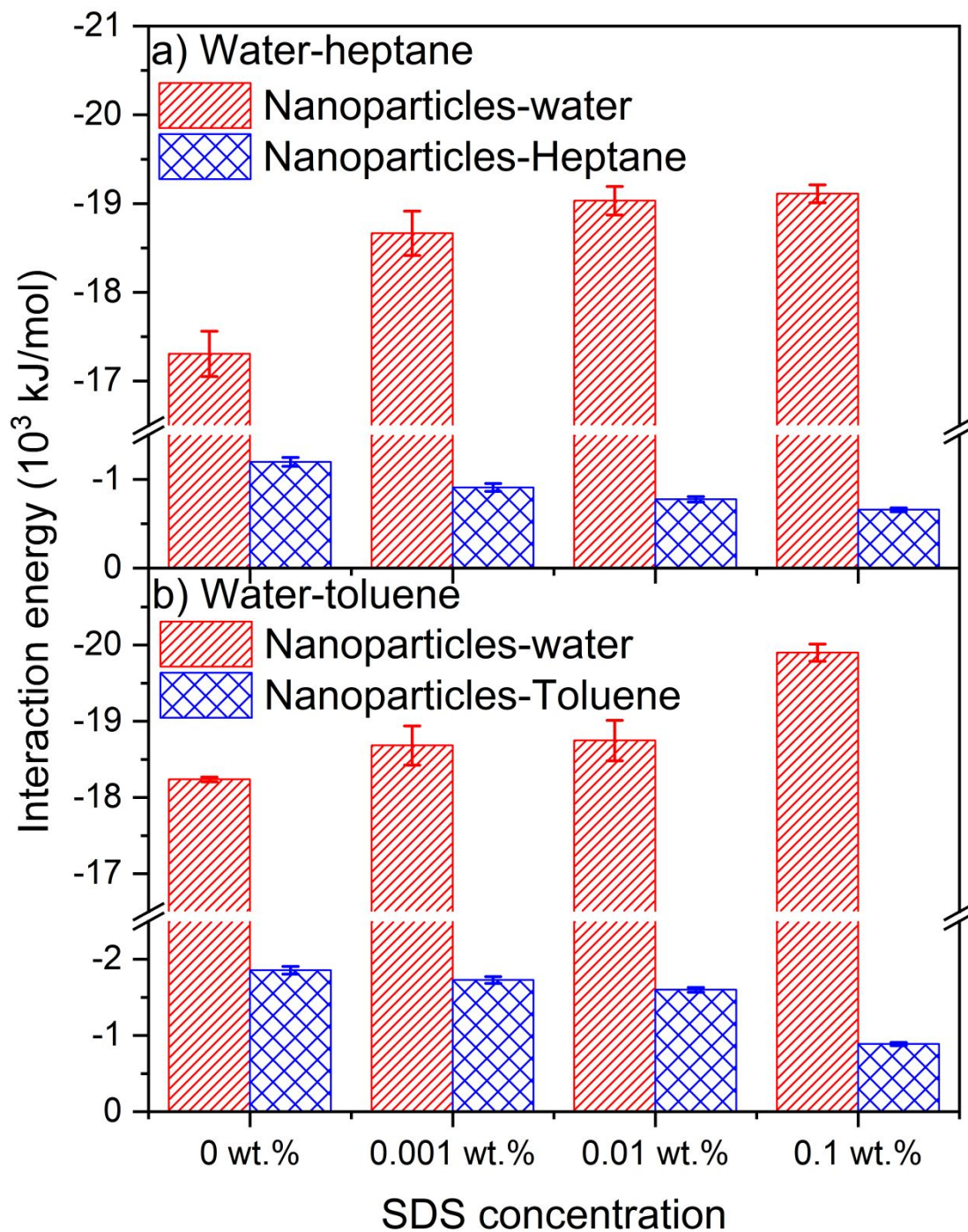
Figure 8. The interfacial tension of water-heptane and water-toluene emulsions in the absence and presence of silica nanoparticles as a function of SDS concentrations. The interfacial tensions are averaged over the last 10 ns of the simulation time. The error bars represent the standard deviation from the mean value of three different simulations.



1

2 **Figure 9.** The aggregation number of silica nanoparticles in (A) water-heptane and (B) water-
 3 toluene emulsions as a function of the SDS concentration. The assembly of SDS molecules at (C)
 4 water-heptane and (D) water-toluene interfaces are characterized by calculating the average
 5 aggregation number of SDS molecules at a concentration of 0.01 and 0.1 wt%. (E) Schematics
 6 show the interfacial configurations of silica nanoparticles and SDS surfactant at water-
 7 hydrocarbons interfaces at different SDS concentrations.

8



1
 2 **Figure 10.** The intermolecular interaction of nanoparticles with (a) water and heptane in water-
 3 heptane emulsion and (b) water and toluene in water-toluene emulsion as a function of the SDS
 4 concentrations. The intermolecular interactions are averaged over the last 10 ns of the simulation
 5 time. The error bars represent the standard deviation from the mean value of three different
 6 simulations.

7
 8